Original Article

Investigating the Effects of Reconstruction Conditions on Image Quality and Radiomic Analysis in Photon-counting Computed Tomography

Miyu Ohata, Ryohei Fukui[1], Yusuke Morimitsu[2], Daichi Kobayashi[2], Takatsugu Yamauchi[2], Noriaki Akagi[2], Mitsugi Honda[2], Aiko Hayashi[3], Koshi Hasegawa, Katsuhiro Kida[1], Sachiko Goto[1], Takao Hiraki[4]

Department of Radiological Technology, Graduate School of Health Sciences, Okayama University, [1]Department of Radiological Technology, Faculty of Health Sciences, Okayama University, [2]Division of Radiological Technology, Okayama University Hospital, [4]Department of Radiology, Faculty of Medicine, Dentistry and Pharmaceutical, Okayama University, Okayama, [3]Department of Radiology, Hiroshima University Hospital, Hiroshima, Japan

Abstract

Introduction: Photon-counting computed tomography (CT) is equipped with an adaptive iterative reconstruction method called quantum iterative reconstruction (QIR), which allows the intensity to be changed during image reconstruction. It is known that the reconstruction conditions of CT images affect the analysis results when performing radiomic analysis. The aim of this study is to investigate the effect of QIR intensity on image quality and radiomic analysis of renal cell carcinoma (RCC). **Materials and Methods:** The QIR intensities were selected as off, 2 and 4. The image quality evaluation items considered were task-based transfer function (TTF), noise power spectrum (NPS), and low-contrast object specific contrast-to-noise ratio (CNR_{LO}). The influence on radiomic analysis was assessed using the discrimination accuracy of clear cell RCC. **Results:** For image quality evaluation, TTF and NPS values were lower and CNR_{LO} values were higher with increasing QIR intensity; for radiomic analysis, sensitivity, specificity, and accuracy were higher with increasing QIR intensity. Principal component analysis and receiver operating characteristics analysis also showed higher values with increasing QIR intensity. **Conclusion:** It was confirmed that the intensity of the QIR intensity affects both the image quality and the radiomic analysis.

Keywords: Image quality, photon-counting computed tomography, quantum iterative reconstruction, radiomics, renal cell carcinoma

Received on: 08-07-2024 **Review completed on:** 11-11-2024 **Accepted on:** 19-01-2025 **Published on:** 24-03-2025

Introduction

Treatment planning for patients with cancer is frequently based on the evidence recommended by relevant academic societies at that time. In recent years, however, attempts have been made to personalize the medical treatment by predicting the prognosis of each patient based on the patient's blood, tissue, imaging, and genetic information, also known as precision medicine.[1] A biopsy of cancer tissue, which is a highly invasive procedure, is essential for precision medicine; however, gene mutations with both good and poor prognoses may coexist in the same cancer tissue.[2] Recently, radiomics, a new image analysis technique, has begun to garner attention.[3] Radiomic analysis involves the measurement of features related to lesion shape, histogram, and texture from the pixel values of the tissues and lesions depicted in computed tomography (CT) and magnetic resonance imaging scans and constructs the predictive models using features that are highly correlated with the histology and genotype of a specific cancer. There are many reports on the usefulness of radiomics, particularly for lung cancer, brain tumors, and breast cancer.[4-6] There have also been reports on the construction of survival prediction models based on the analysis of the relationship between the cancer features and survival.[7,8]

Renal cell carcinoma (RCC) is caused by the cancerous transformation of renal tubular epithelial cells and is distinct from renal pelvis cancer. It accounts for 2% of all cancer cases in Japan, with a male-to-female ratio of 2:1 and a higher

Access this article online

Quick Response Code:

Website: www.jmp.org.in

DOI: 10.4103/jmp.jmp_114_24

Address for correspondence: Dr. Ryohei Fukui, Department of Radiological Technology, Faculty of Health Sciences, Okayama University, 2-5-1, Shikatacho, Kitaku, Okayama 700-8558, Japan. E-mail: rfukui@okayama-u.ac.jp

How to cite this article: Ohata M, Fukui R, Morimitsu Y, Kobayashi D, Yamauchi T, Akagi N, *et al*. Investigating the effects of reconstruction conditions on image quality and radiomic analysis in photon-counting computed tomography. J Med Phys 2025;50:100-7.

incidence after the age of 40, as well as in people in their 60s to 70s.[9] RCC can be classified according to histological type, such as clear cell RCC (ccRCC) and chromophobe RCC, with ccRCC accounting for 70% of all cases.[10] A diagnosis of RCC is often confirmed by imaging studies; however, in cases in which the histological type cannot be determined, a tissue biopsy is performed, and the histological type is confirmed through the pathological diagnosis. There are many reports on the utilization of radiomic analysis in RCC, and the classification of histological type, degree of invasion, and grading has been achieved with high accuracy.[11-13]

Photon-counting CT (PCCT), another diagnostic option, started to be used clinically in Japan in 2021. While conventional CT utilizes a method in which every X-ray energy incident on the detector is integrated to form an image, PCCT forms images by counting the number of X-ray photons per the unit of energy. Energy-differentiated images can be easily obtained; therefore, with the benefits of producing higher resolution and lower exposure.[14] Due to the difference in the method of X-ray detection, PCCT also utilized a different method for reconstruction than conventional CT. One of these methods is quantum iterative reconstruction (QIR), which can be set as any one of five steps – from 0 to 4 – and can be set when reconstructing the image. There are no reports, however, on the effects of changing QIR intensity on radiomic analysis. The present study, therefore, aimed to investigate the effects of QIR intensity on physical image quality and radiomic analysis.

Materials and Methods

Methods

This paper outlines of image quality assessment and radiomic analysis for RCC are shown in Figure 1.

Materials

In the present study, we performed a physical evaluation of image quality as well as the radiomic analysis. All CT images were acquired using a PCCT system (NAEOTOM Alpha; Siemens Healthcare Co., Tokyo, Japan). A solid rod (iodine 2 mg/mL, 28 mm diameter) within a multi-energy CT phantom (Sun Nuclear, FL, USA) was used to assess the image quality, as the CT value of this rod has a CT value comparable to that of the renal parenchyma. An X-ray water phantom model was used for the chest and abdomen (Water Phantom, Kyoto Kagaku, Kyoto, Japan), and a base supporting the solid rod was created using a three-dimensional (3D) printer (Saturn2; ELEGO, Shenzhen, China). CTmeasureBasic (v0.97b2), distributed by the Japanese Society of CT Technology, was used to perform the physical evaluation.[15] For the radiomic analysis, we utilized 3D Slicer (v5.2.1) for lesion segmentation, Google Colaboratory as the Python-based execution environment for feature calculation, and PyRadiomics, a Python package, for feature extraction. RStudio (v2023.12.0 + 369) was used for the statistical analysis.

Imaging and reconstruction conditions

We selected the following imaging parameters, typically utilized for routine imaging of the kidneys at (The name of the author's institution will be included) University Hospital: tube voltage, 140 kV; CT automatic exposure control was used; ref. mAs, the noise index of PCCT, 145 mAs (recommended value of CT equipment manufacturer); rotational speed, 0.5 s; pitch factor, 0.8; field of view, 320 mm; and dose-length product, 62.5 mGy-cm when acquiring images for image quality evaluation, although it varied from case to case among the scans evaluating the kidney. The reconstruction conditions were the same for both image quality assessment and radiomic analysis. The T3D reconstruction method was selected for the present study, as it corresponds to the reconstructions performed in conventional energy-integrated CT and uses all of the acquired X-ray quantum energies for the reconstruction. The QIR of interest in the present study can be set in one of five steps, from 0 (off) to 4. The larger the QIR value, the greater the number of iterations. For the present study we selected, off,

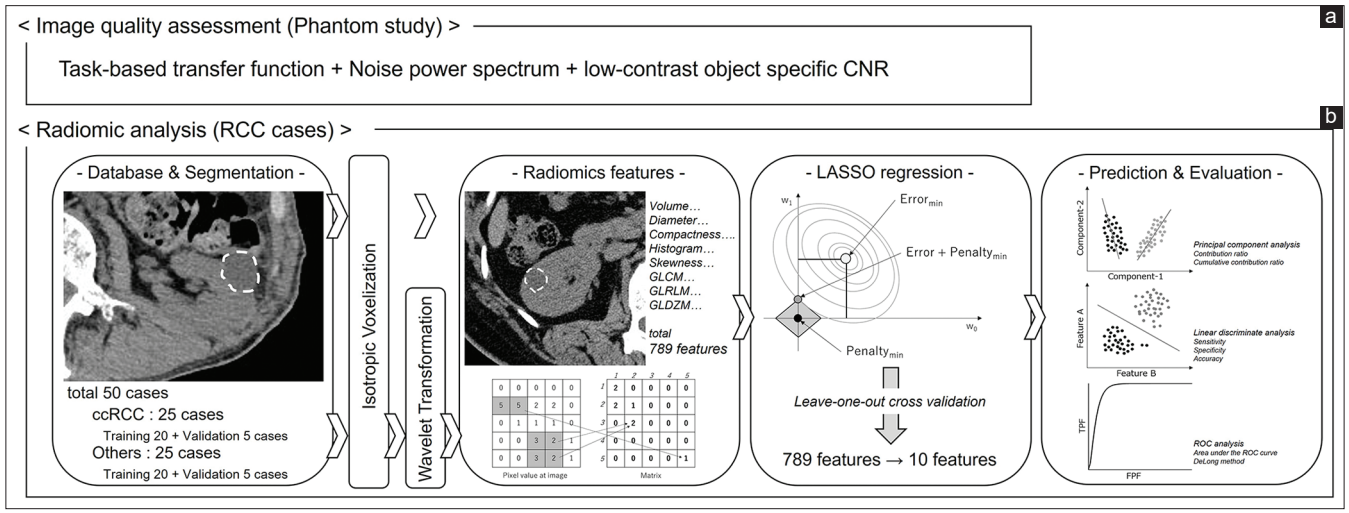

Figure 1: Outlines for (a) Image quality assessment using handmade phantom and (b) Radiomics analysis using renal cell carcinoma cases. RCC: Renal cell carcinoma, CNR: Contrast-to-noise ratio, LASSO: Least absolute shrinkage and selection operator

2, and 4 for evaluation. For the reconstruction function, Br44 was selected as a soft-tissue function, and the slice thickness and spacing were both set to 1.0 mm.

Handmade phantom and image quality assessment

A schematic of the handmade phantom used for the image quality assessment, which mimicked the renal parenchyma by fixing a solid rod slightly to the lower right of a water-filled phantom, is shown in Figure 2. A 3D printer was used to create a base to support the solid rod, as contact between the rod and the phantom wall would make analysis difficult with the solid rod submerged in the water phantom. A total of 500 CT images were collected for the present study by obtaining 25-mm images along the direction of the long axis of the solid rod and repeating this process 20 times. Figure 3 shows the CT images of handmade phantom used in the present analysis; however, the images were not additionally averaged.

Task-based transfer function (TTF), noise power spectrum (NPS), and low-contrast object-specific contrast-to-noise ratio (CNR_{LO}) were used to assess the image quality. TTF was calculated using the solid rod with the circular edge method.[16] As a CNR of ≥28 for the rod is recommended for sufficient accuracy in TTF measurements, the TTF was calculated from an additive average of 500 images.[17] NPS was calculated using the radial frequency method from the uniform images obtained by placing a 128 × 128 pixel region of interest (ROI) in an area of the handmade phantom with water but no solid rods. The average NPS was calculated from the NPSs obtained from the same slice 20 times. The method for determining CNR_{LO} was as follows: first, the $\bar{u}$ value, which represents spatial frequency, was calculated from the diameter of the solid rod using the following equation:

$$\bar{u}^2 = \frac{\int_0^\infty u^2 \mid S(u) \mid^2 du}{\int_0^\infty \mid S(u) \mid^2 du} \quad (1),$$

with $S(u)$ calculated from the following equation:

$$S(u) = \frac{J_1(\pi du)}{2\pi du} \quad (2),$$

where J_1 is the Bessel function, d is the rod diameter, and u is the spatial frequency. The NPS value corresponding to this $\bar{u}$ value was used to calculate CNR_{LO} using the following formula:

$$CNR_{LO} = \frac{ROI_S - ROI_B}{\sqrt{NPS(\bar{u})}} \quad (3),$$

In which ROI_S represents the CT value of the rod, ROI_B represents the CT value of the background and NPS($\bar{u}$) represents the NPS value at values.

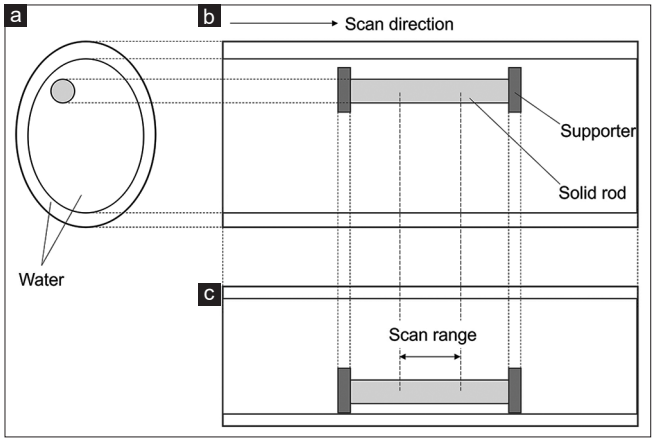

Figure 2: Schematic diagrams and computed tomography images of the handmade water phantom from (a) Frontal side, (b) Upper side and (c) Lateral side. The phantom is filled with water. The solid rod is placed in the lower right-hand corner of the phantom to mimic the position of the kidney

Database and segmentation for radiomic analysis

A total of 50 cases (31 males; mean age, 66.9 ± 10.1 years) who underwent PCCT for the treatment of renal disease at (the name of the author's institution will be included) University Hospital between May 2023 and March 2024 were included in the present study. Of the 50 cases, 25 were ccRCCs and the remaining 25 were neoplastic lesions (others), including RCCs other than ccRCCs, chromophobe RCCs, papillary RCCs, angiomylipomas, and oncocytic neoplasias. Of these 25 cases, 20 were used to build a prediction model (training data), and the remaining five cases were used for validation (validation data). The pathological diagnoses of all of the cases were confirmed by renal biopsy. Contrast enhancement studies were performed in all cases; however, noncontrast images were used for radiomic analysis to eliminate any influence of the contrast media. Images were output in Digital Image and Communications in Medicine format, and the use of these clinical images was approved by the Ethical Review Committee of (The name of the author's institution will be included) University School of Medicine (no. K2305-033).

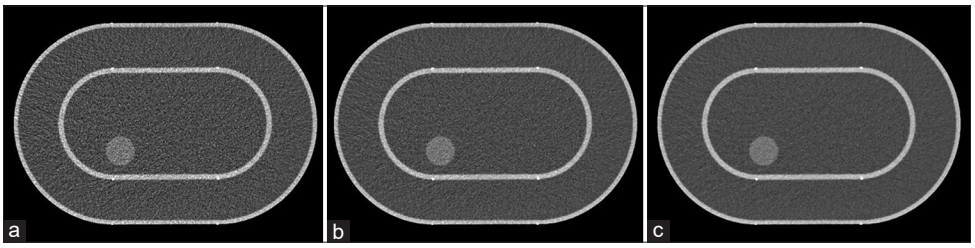

Figure 3: Samples of the axial computed tomography image with quantum iterative reconstruction intensities of (a) off, (b) 2, and (c) 4

Freehand segmentation of the renal lesions was performed by one of the coauthors (a radiological technologist with 14 years of experience) using 3D Slicer, and the confirmed and revised with the remaining coauthors. Segmentation was performed using only one slice where the largest tumor diameter is depicted. The extent of the tumor was determined by referring to the contrast-enhanced CT images taken at the same time to mark the ROI, and the segmentation results were output in nearly raw raster data format. Incidentally, as the extent of the renal tumor was the same in each slice, even if the QIR intensity was different, the ROI set in QIR_4 was shared as a segmentation for other images with QIR intensities.

Radiomics features and least absolute shrinkage and selection operator regression

Isotropic voxelization was performed as a preprocessing step before the features were measured. In the CT images, the sample size was consistent in the xy-plane, although that in the z-axis direction, which corresponds to the slice thickness, was not. Because the sampling interval in the xyz direction was assumed to be equal for feature measurements, it was necessary to equalize the sampling interval in the xyz direction by isotropic voxelization.[18] In addition, a dataset with a wavelet transform was also created. The wavelet transform allows more features to be obtained by decomposing the image into low- and high-frequency components using low- and high-pass filters, respectively, which can detect image features that emphasize noise and edge components.[19] A total of 789 radiomics features related to shape, size, signal intensity, texture, and wavelet transform were measured from the tumor area specified during segmentation. A large number of features, however, can easily lead to overfitting when building a predictive model; therefore, feature dimensionality was reduced using least absolute shrinkage and selection operator (LASSO) regression,[20] as follows:

$$E = \frac{1}{2}\Sigma(y_i - w_i x_i)^2 + \lambda\sum_{i=1}^{n}|w_i| \quad (4),$$

Where E is the error, y_i is the correct value, $w_i x_i$ is the prediction and λ is the regularization parameter. The minimum value of λ was calculated using leave-one-out cross-validation method. In addition, by adjusting the value of λ, it is possible to change the number of selected radiomics features. In the present study, the value of the regularization parameter λ was adjusted so that the number of selected features was 10 for each QIR intensity.

Prediction and evaluation

A predictive model for discriminating RCC was constructed and evaluated using the features selected through the LASSO regression. Principal component analysis (PCA), Fisher's linear discriminant analysis (LDA), and receiver operating characteristic (ROC) analysis were used for the construction and evaluation of the predictive model. PCA is a statistical approach that aims to reduce the number of variables by aggregating the information held by highly correlated variables, making it easier to interpret the features of the data.[21] The ten selected features were compressed to two dimensions (first and second principal components), and the cumulative contribution ratio of each principal component were calculated and compared among the QIR intensities.

To visualize the usefulness of the selected features in LDA, decision boundaries were obtained using two features that were highly correlated with the tissue type, while the sensitivity, specificity, and accuracy were obtained using the decision boundaries. Furthermore, the validation data, which were not used in the construction of the predictive model, were fitted to this discriminant boundary, and the sensitivity, specificity, and accuracy were also determined.

Results

Image quality assessment

Figure 4a shows that TTF decreased as the QIR intensity increased; however, the difference decreased at higher frequencies and exhibited similar values. The TTF at 0.1 cycles/mm was 0.54, 0.48, and 0.44 for QIR_off, 2 and 4, respectively.

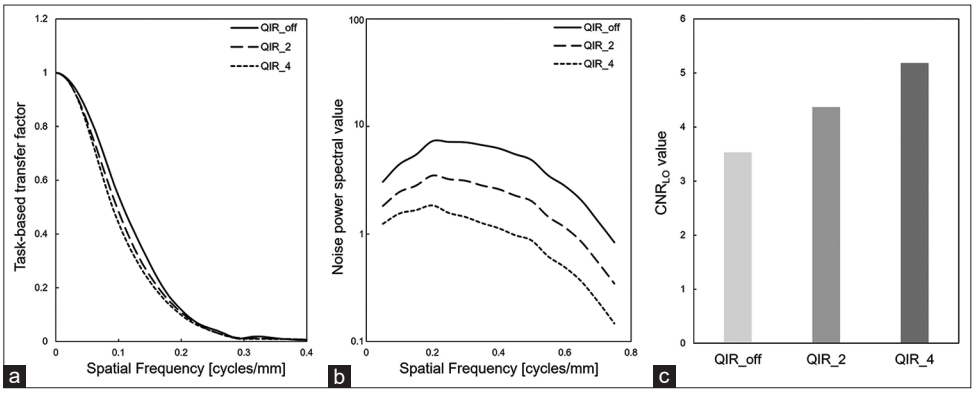

Figure 4: Results of the (a) TTF, (b) Noise power spectrum (NPS) and (c) Low-contrast object specific contrast-to-noise ratio (CNR_{LO}) in various quantum iterative reconstruction (QIR) intensities. The TTF at 0.1 cycles/mm was 0.54, 0.48, and 0.44 for QIR_off, 2 and 4 respectively. The NPS values decreased as the QIR intensity increased. The CNR_{LO} was higher with increasing QIR intensity. CNR_{LO}: Low-contrast object specific contrast-to-noise ratio, QIR: Quantum iterative reconstruction

The NPS results are presented in Figure 4b, which shows that NPS values decreased as the QIR intensity increased. All NPSs were highest at a spatial frequency of 0.2 cycles/mm, with an average noise frequency of 0.316 ± 6.0%; the shape of the NPSs was similar, although with lower values at higher frequencies. The CNR_{LO} results are presented in Figure 4c, the CNR_{LO} was higher with increasing QIR intensity.

Results of least absolute shrinkage and selection operator regression

Figure 5 shows ccRCCs and values by QIR intensity, and features extracted by the LASSO regression are listed in Table 1. The features obtained by the wavelet transform (wavelet) were selected for all QIR intensities. Textural features (e.g., glcm, gldm, and glszm) were selected most frequently, followed by statistical features (first-order). No shape features were selected. An explanation is provided only for the features used in LDA, which are described below. In the texture features, "GrayLevelNonUniformity" indicates the similarity of pixel values within the ROI, "ClusterShade" indicates the skewness and uniformity in glcm, "DependenceNonUniformity" is a similarity measure for pixel value dependence, and "DependenceNonUniformityNormalised" is a normalized version of this.

Results of principal component analysis, linear discriminant analysis, and receiver operating characteristic

The results of the contribution and cumulative contribution rates for each QIR intensity calculated by PCA are presented in Table 2; the higher the intensity of the QIR, the higher the value of both indicators.

The LDA results for the training and validation data at each QIR intensity are shown in Figure 6. The sensitivity, specificity, and accuracy calculated using the decision boundaries of the LDA are presented in Table 3. The higher the QIR intensity, the higher the sensitivity, specificity, and accuracy. Compared with the training data, the indices for the validation data were smaller.

The AUC results for each QIR intensity are presented in Figure 7, with AUCs of 0.70, 0.73, and 0.75 for QIR_off, 2, and 4, respectively.

Discussion

In the present study, we investigated the effects of QIR intensity, an adaptive iterative reconstruction method in PCCT, on image quality and radiomic analysis. In the image quality assessment, NPS remained shaped consistently, even when the QIR intensity was changed; therefore, no effects on the frequency response were observed. TTF was slightly reduced, which can be attributed to noise reduction and smoothing; however, it did not decrease significantly, and the values were identical at high frequencies, indicating that the resolution characteristics were maintained even when the QIR intensity was changed. Previous studies have reported that the average and peak noise frequencies are almost the same for all reconstructions, and that the noise can be reduced without affecting the noise texture by increasing the intensity of the QIR.[21,22] It has also been reported that one of the main objectives of QIR is to reduce image noise without affecting the noise texture and structure resolution properties,[23] consistent with the results of the present study. The solid rod used in the present study, however, had a diameter of 28 mm, allowing for a task-based analysis mimicking the size of the kidney. Therefore, one limitation of the present study is that this was not a task-based analysis of RCC, which is often smaller than a kidney. CNR_{LO} increased as QIR intensity increased; however, it is assumed that the NPS value, the denominator of the CNR_{LO}, has a greater influence than the

Table 1: Radiomic features selected by the least absolute shrinkage and selection operator regression

	QIR intensity		
	Off	**2**	**4**
Radiomic features	wavelet-LLH_firstorder_Maximum	wavelet-LHH_firstorder_Mean	wavelet-LLH_firstorder_Skewness
	wavelet-LLH_glszm_LargeAreaEmphasis	wavelet-LHH_glcm_ClusterShade	wavelet-LHH_firstorder_MeanAbsoluteDeviation
	wavelet-LHH_glcm_ClusterShade	wavelet-LHH_glrlm_HighGrayLevelRunEmphasis	wavelet-LHH_firstorder_Median
	wavelet-LHH_glrlm_HighGrayLevelRunEmphasis	wavelet-HLL_glcm_Correlation	wavelet-LHH_glrlm_HighGrayLevelRunEmphasis
	wavelet-HLL_firstorder_Energy	wavelet-HLH_firstorder_Entropy	wavelet-LHH_glrlm_LowGrayLevelRunEmphasis
	wavelet-HLL_glszm_ZoneEntropy	wavelet-HLH_firstorder_Median	wavelet-LHH_glszm_LargeAreaHighGrayLevelEmphasis
	wavelet-HLL_gldm_SmallDependenceLowGrayLevelEmphasis	wavelet-HLH_firstorder_Uniformity	wavelet-HLL_glcm_Correlation
	wavelet-HLH_firstorder_Median	wavelet-HLH_glrlm_LongRunHighGrayLevelEmphasis	wavelet-HLH_glrlm_LongRunHighGrayLevelEmphasis
	wavelet-HLH_firstorder_Minimum	wavelet-HLH_glszm_ZoneVariance	wavelet-HHL_gldm_DependenceNonUniformity
	wavelet-HLH_glszm_GrayLevelNonUniformity	wavelet-HLH_gldm_GrayLevelVariance	wavelet-HHL_gldm_DependenceNonUniformityNormalized

QIR: Quantum iterative reconstruction

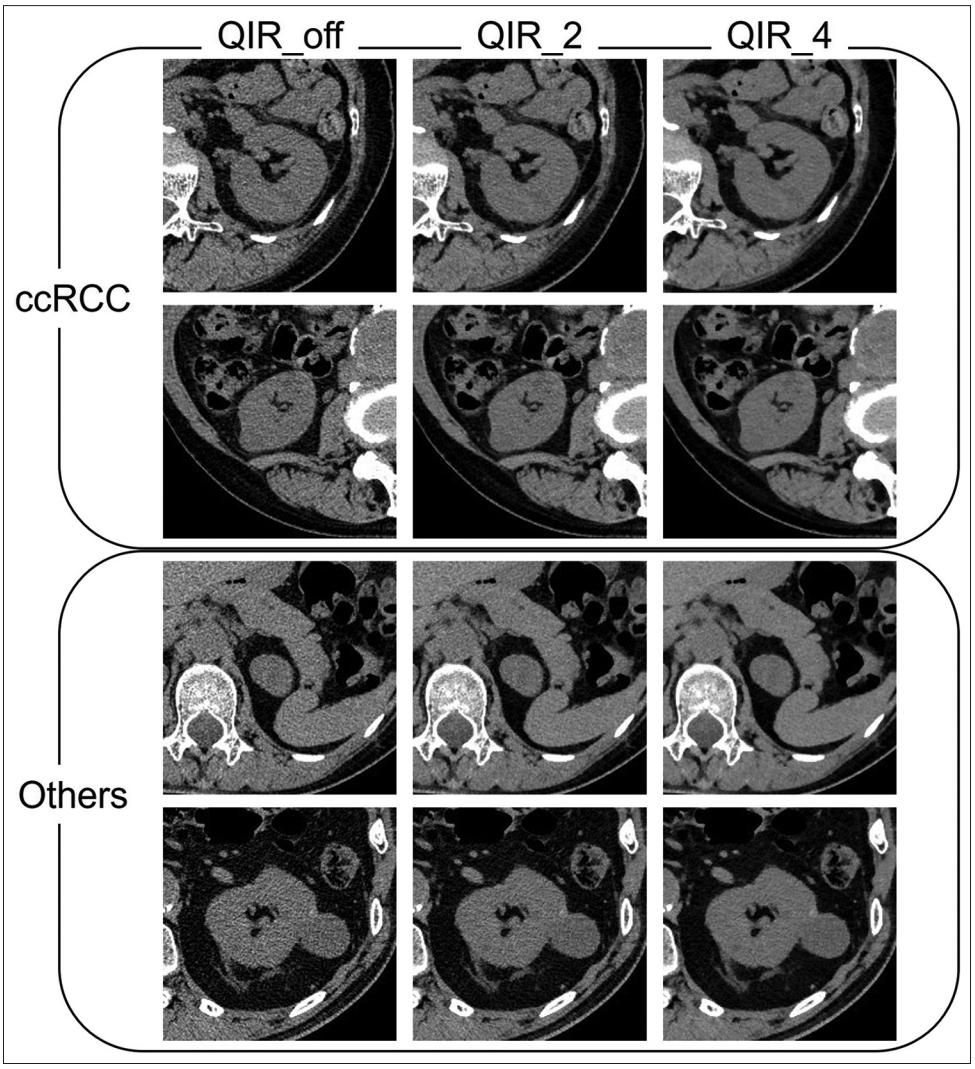

Figure 5: Samples of the case used for radiomics analysis. In "Others" case, the upper row is the papillary renal cell carcinoma (RCC) and the lower row is the chromophobe RCC. QIR: Quantum iterative reconstruction

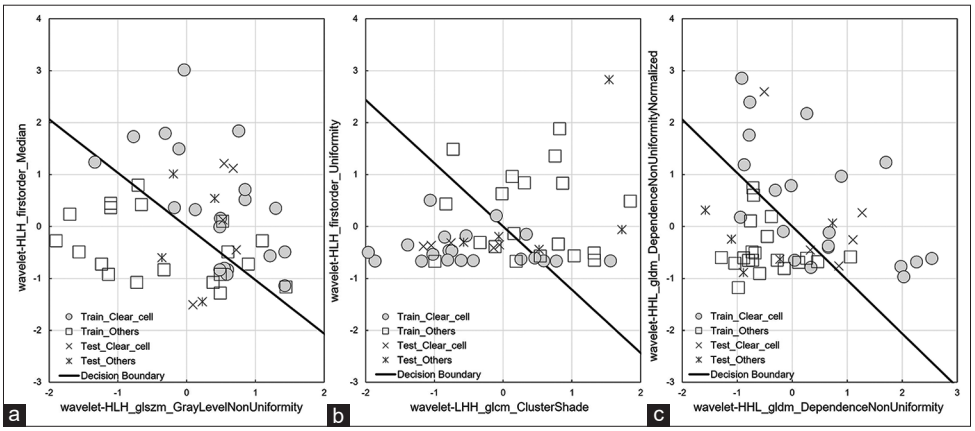

Figure 6: Results of linear discriminant analysis with (a) QIR_off, (b) QIR_2, and (c) QIR_4. The sensitivity and specificity of training data were 0.75/0.75, 0.75/0.80 and 0.80/0.90 in the order of quantum iterative reconstruction intensities

contrast between the solid rod and background. There have been several reports on the subjective evaluation of images using modified QIR; however, there are varying reports on observer studies of image quality, indicating that QIR_3 is optimal all around,[23] or QIR_4 for the portal vein and QIR_3 for the lungs.[21,22] The results of image quality assessments

Table 2: Results of the principal component analysis

Contribution ratio	QIR intensity		
	Off	2	4
1st component	0.44	0.53	0.50
2nd component	0.21	0.19	0.28
Cumulative contribution ratio	0.65	0.72	0.78

PCA: Principal component analysis, QIR: Quantum iterative reconstruction

Table 3: Results of sensitivity, specificity, and accuracy obtained from the linear discriminant analysis

	QIR intensity					
	Off		2		4	
	Train	Test	Train	Test	Train	Test
Sensitivity	0.75	0.80	0.75	1.0	0.80	0.80
Specificity	0.75	0.60	0.80	0.60	0.90	0.80
Accuracy	0.75	0.67	0.79	0.71	0.89	0.80

LDA: Linear discriminant analysis, QIR: Quantum iterative reconstruction

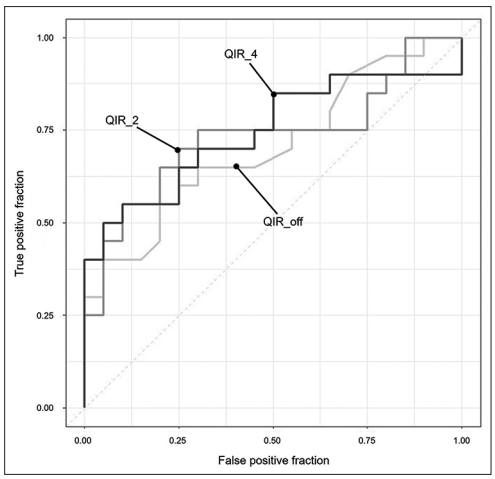

Figure 7: Results of receiver operating characteristic analysis. The area under the curves of QIR_off, _2 and _4 were 0.70, 0.73, and 0.75, respectively. QIR: Quantum iterative reconstruction

and observer studies may differ in the kidney, which is the subject of the present study, and should be investigated in the future. In addition, manual segmentation is affected if the lesion visibility changes depending on QIR intensity, as the shape of the ROI may differ depending on the QIR intensity in a given case. In the present study, however, the ROI was set on the image set by QIR_4, and utilized by QIR_off and QIR_2. Therefore, we believe that segmentation had no effect.

From the 789 features obtained in the present study, after adjusting λ, that number was reduced to 10. All of the selected features were those to which the wavelet transform was added. We believe that the addition of the wavelet transform, therefore, facilitates the description of RCC histology because it allows for a more diverse representation. The PCA using the features extracted at each QIR intensity showed that the cumulative contribution to the second principal component was higher when the QIR intensity was higher. In the radiomic analysis of positron emission tomography images, it has been reported that image noise directly affects the reproducibility of radiomic features, and that reducing the noise results in significant feature agreement,[24] indicating that the feature values change with image noise. We believe, therefore, that the reduction of noise increases the discrimination accuracy of the predictive model using the features, which was also evident from the cumulative contribution ratios.

When decision boundaries were set using the top 2 highly correlated features of the 10 features obtained by LASSO regression, the higher the QIR Intensity, the higher the sensitivity, specificity, and accuracy, while the lower values of these indices in the validation dataset were attributed to the small number of cases. The AUC obtained from the ROC curve analysis improved with increasing QIR intensity. In the present study, the cases were collected retrospectively; however, there were very few cases in which PCCT was performed, and the pathological diagnosis was confirmed by renal biopsy. Future studies are needed to determine the number of cases, for example, in collaborative studies conducted at other centers. The present study was included only RCC cases; therefore, other sites and diseases are unknown.

Conclusion

The effects of changing the intensity of QIR, an adaptive iterative reconstruction method used in PCCT, on image quality and radiomic analysis were elucidated in the present study: QIR_4 was able to reduce noise while maintaining resolution characteristics. In addition, in the Radiomics analysis targeting ccRCC, the QIR_4 prediction model showed a cumulative contribution rate of 0.78, with sensitivity, specificity, and accuracy all exceeding 0.8, indicating high prediction accuracy. Therefore, in the radiomics analysis of RCC, it is necessary to consider that the intensity of QIR affects the prediction accuracy. Further studies, however, with a larger number of cases are required before it can be concluded that QIR_4 is the best model for radiomic analysis.

Financial support and sponsorship

Nil.

Conflicts of interest

There are no conflicts of interest.

References

1. Baumann M, Krause M, Overgaard J, Debus J, Bentzen SM, Daartz J, *et al.* Radiation oncology in the era of precision medicine. Nat Rev Cancer 2016;16:234-49.
2. Gerlinger M, Rowan AJ, Horswell S, Math M, Larkin J, Endesfelder D, *et al.* Intratumor heterogeneity and branched evolution revealed by multiregion sequencing. N Engl J Med 2012;366:883-92.

3. Mayerhoefer ME, Materka A, Langs G, Häggström I, Szczypiński P, Gibbs P, *et al.* Introduction to radiomics. J Nucl Med 2020;61:488-95.
4. Wilson R, Devaraj A. Radiomics of pulmonary nodules and lung cancer. Transl Lung Cancer Res 2017;6:86-91.
5. Brancato V, Cerrone M, Lavitrano M, Salvatore M, Cavaliere C. A systematic review of the current status and quality of radiomics for glioma differential diagnosis. Cancers (Basel) 2022;14:2731.
6. Zheng X, Yao Z, Huang Y, Yu Y, Wang Y, Liu Y, *et al.* Deep learning radiomics can predict axillary lymph node status in early-stage breast cancer. Nat Commun 2020;11:1236.
7. Li G, Li L, Li Y, Qian Z, Wu F, He Y, *et al.* An MRI radiomics approach to predict survival and tumour-infiltrating macrophages in gliomas. Brain 2022;145:1151-61.
8. Yu Y, Tan Y, Xie C, Hu Q, Ouyang J, Chen Y, *et al.* Development and validation of a preoperative magnetic resonance imaging radiomics-based signature to predict axillary lymph node metastasis and disease-free survival in patients with early-stage breast cancer. JAMA Netw Open 2020;3:e2028086.
9. Morita J, Matsui H, Ogawa H. Frontiers of renal cell carcinoma treatment. J Showa Med Univ 2016;76:98-107. [in Japanese].
10. El-Zaatari ZM, Truong LD. Renal cell carcinoma in end-stage renal disease: A review and update. Biomedicines 2022;10:657.
11. Mühlbauer J, Egen L, Kowalewski KF, Grilli M, Walach MT, Westhoff N, *et al.* Radiomics in renal cell carcinoma-a systematic review and meta-analysis. Cancers (Basel) 2021;13:1348.
12. Yang L, Gao L, Arefan D, Tan Y, Dan H, Zhang J. A CT-based radiomics model for predicting renal capsule invasion in renal cell carcinoma. BMC Med Imaging 2022;22:15.
13. Yi X, Xiao Q, Zeng F, Yin H, Li Z, Qian C, *et al.* Computed tomography radiomics for predicting pathological grade of renal cell carcinoma. Front Oncol 2020;10:570396.
14. Esquivel A, Ferrero A, Mileto A, Baffour F, Horst K, Rajiah PS, *et al.* Photon-counting detector CT: Key points radiologists should know. Korean J Radiol 2022;23:854-65.
15. Ichikawa K. CTmeasure. Available from: https://www.jsct-tech.org/,2012-2014. [Last accessed on 2023 Sep 10].
16. Takata T, Ichikawa K, Mitsui W, Hayashi H, Minehiro K, Sakuta K, *et al.* Object shape dependency of in-plane resolution for iterative reconstruction of computed tomography. Phys Med 2017;33:146-51.
17. Urikura A, Ichikawa K, Hara T, Nishimaru E, Nakaya Y. Spatial resolution measurement for iterative reconstruction by use of image-averaging techniques in computed tomography. Radiol Phys Technol 2014;7:358-66.
18. Whybra P, Parkinson C, Foley K, Staffurth J, Spezi E. Assessing radiomic feature robustness to interpolation in (18)F-FDG PET imaging. Sci Rep 2019;9:9649.
19. Larue RT, Defraene G, De Ruysscher D, Lambin P, van Elmpt W. Quantitative radiomics studies for tissue characterization: A review of technology and methodological procedures. Br J Radiol 2017;90:20160665.
20. Hastie T, Tibshirani R, Wainwright M. Statistical Learning with Sparsity: The Lasso and Generalizations. 1st ed. New York: CRC Press; 2015. p. 2-10.
21. Sartoretti T, Racine D, Mergen V, Jungblut L, Monnin P, Flohr TG, *et al.* Quantum iterative reconstruction for low-dose ultra-high-resolution photon-counting detector CT of the lung. Diagnostics (Basel) 2022;12:522.
22. Sartoretti T, Landsmann A, Nakhostin D, Eberhard M, Roeren C, Mergen V, *et al.* Quantum iterative reconstruction for abdominal photon-counting detector CT improves image quality. Radiology 2022;303:339-48.
23. Sartoretti T, McDermott M, Mergen V, Euler A, Schmidt B, Jost G, *et al.* Photon-counting detector coronary CT angiography: Impact of virtual monoenergetic imaging and iterative reconstruction on image quality. Br J Radiol 2023;96:20220466.
24. Keller H, Shek T, Driscoll B, Xu Y, Nghiem B, Nehmeh S, *et al.* Noise-based image harmonization significantly increases repeatability and reproducibility of radiomics features in PET images: A phantom study. Tomography 2022;8:1113-28.